Electrical control of magnetic quantum wells: Monte Carlo simulations

E. Dias Cabral, M. A. Boselli, R. Oszwałdowski, I. Žutić, and I. C. da Cunha Lima

Phys. Rev. B **84**, 085315 — Published 26 August 2011

DOI: 10.1103/PhysRevB.84.085315

Electrical Control of Magnetic Quantum Wells - Monte Carlo Simulations

E. Dias Cabral,[1] M. A. Boselli,[2] R. Oszwałdowski,[3,4] I. Žutić,[3] and I. C. da Cunha Lima[5]

[1] *Tecnologia em Polímeros Universidade Estadual da Zona Oeste. Rio de Janeiro, RJ 23070-200 Brasil*
[2] *Instituto de Física, Universidade Federal de Uberlândia, Uberlândia, MG, 38400-902, Brazil.*
[3] *University at Buffalo, State University of New York, Buffalo, NY 14260, USA*
[4] *Institute of Physics, N. Copernicus University, Toruń, Poland*
[5] *Instituto de Física, Universidade do Estado do Rio de Janeiro, Rio de Janeiro, RJ 20500-013, Brazil*

We use Monte Carlo simulations to analyze electric-field control of Curie temperature T_C for carrier-mediated ferromagnetism in semiconductors. Gating employed to achieve electrostatic doping in optimized geometry of (Ga,Mn)As, a prototypical ferromagnetic semiconductor, reveals a highly-tunable ferromagnetic order. We show the feasibility of $\Delta T_C > 100$ K, an order of magnitude greater then the state-of-the-art measurements, at fields substantially smaller then the breakdown values. Such controllable ferromagnetism may help elucidate the mechanism of carrier-mediated magnetism in various semiconductors and offer versatile spintronic applications.

PACS numbers: 75.50.Pp, 75.30.Hx, 75.70.Ak

I. INTRODUCTION

Carrier-mediated magnetism in dilute magnetic semiconductors (DMS) offers a versatile control of the exchange interaction between carriers and magnetic impurities. The onset of ferromagnetism and the corresponding change in the Curie temperature (T_C) can be achieved by increasing the carrier density using an applied electric field, photo-excitations, or even heating.[1–7]

The use of electric field for a reversible electrostatic doping in DMS is particularly suitable, since it does not alter the level of disorder,[8] while providing important clues about the origin of magnetic ordering, including the possibility of the impurity band formation and localization effects,[9–13] and offering additional opportunities for spintronic devices.[3] Moreover, the attainable electric field[14] can also strongly modify materials properties in other systems such as high-temperature superconductors, manganites, and single molecule devices.[8,15]

Typically, DMS are Mn-doped III-V or II-VI materials,[3,16,17] while most of the measurements of the electric field effects were performed in two-dimensional (2D) DMS structures: quantum wells (QWs) and thin layers. The pioneering experiments probing the role of electric field in (In,Mn)As were limited to low temperature, $T_C \sim 25$ K, and a small variation $\Delta T_C \sim 1$ K, requiring a large gate voltage $V_G \sim 100$ V in a field effect transistor (FET) geometry. However, the subsequent advances in (Ga,Mn)As have shown $T_C > 100$ K, $\Delta T_C > 10$ K, and $V_G < 10$ V (Ref.18–22) including controlling T_C even at room temperature in GaSb/Mn digital alloys.[23]

In this work, we focus on (Ga,Mn)As, an extensively studied material,[16,24] reported to have a significantly higher $T_C \sim 250$ K for GaAs films with Mn δ-doping[25] than in thin (Ga,Mn)As layers ($T_C < 200$ K).[26,27] Our goal is to, using (Ga,Mn)As-based parameters, provide theoretical guidance for optimization of 2D DMS structures, which simultaneously possess a high T_C and allow a high degree of control (large $\Delta T_C/T_C$).

We use an applied electric field for charge/carrier redistribution thus altering the carrier density in the magnetic layer, instead of, as previously considered, providing a source or a drain of carriers inside the QW. This is a substantial difference with the prior experiments,[13,18–22] since once the total charge inside the QW remains constant, while changing the electric field, the effects of disorder on localization will not be substantially affected.

Previous studies of the effect of the electric field in such structures[28,29] employed the effective mass approximation combined with the mean-field approach,[16,30] and neglected any effect of the exchange interaction on carriers. The mean-field approach neglects thermal fluctuations, and disorder (the latter by using Virtual Crystal Approximation).[31–33] For this reason, Monte Carlo (MC) is often preferred over mean-field.[34–37] MC was used to discuss the influence of anisotropy of the exchange interaction in 2D model systems,[38] as well as to simulate realistic 2D systems.[39,40] The latter calculations go beyond the RKKY approach, as the hole states are calculated using actual Mn spins configurations generated in MC. Such an approach is rather demanding computationally, which may limit its modeling capability. Here, we propose a simpler method, which allows optimizing DMS QW structures over a wide range of parameters (such as applied electric fields, positions of $\delta-$layer etc). To make this approach accessible with even modest computer resources, the method does not include potential and magnetic disorder in the plane perpendicular to growth direction.[30]

II. MODEL

In the usual RKKY scheme, the interaction between the hole Fermi gas and the Mn 5/2 spins is treated as a second order perturbation in the Kondo-like exchange $H_{p-d} = -\beta \sum_i \mathbf{S}_i \cdot \mathbf{s}\, \delta(\mathbf{r} - \mathbf{R}_i)$, where the localized spin $\mathbf{S}_i$ of the Mn ion at position $\mathbf{R}_i$ is assumed to be a classical variable, and $\mathbf{s}$ is the spin operator of the carrier at position $\mathbf{r}$; β is the p-d interaction. However, the exchange-

induced splittings in DMS systems can be large with respect to the hole-gas Fermi energy, so that the above RKKY scheme is not reliable in DMS. Our approach goes beyond the usual scheme, since our unperturbed Hamiltonian H_0 [Eq. (1)] contains the mean-field contribution to the exchange interaction. Thus, the spectrum of H_0 already exhibits the exchange splittings.

We introduce the mean-field contribution into H_0 as a $z-$dependent magnetization $V_{\rm mag}^{\rm eff}(z)$ of the Mn ions,[41] on equal footing with the z-dependent potential describing the transverse electric field E. We study a thin GaAs slab of width L, modeled by an infinite QW,[39] and a δ-like (Ga,Mn)As layer of width $w \ll L$, at a distance d off-center, inside the QW (inset in Fig. 1). Controlled placement of the δ-layer have been demonstrated experimentally.[42] The model Hamiltonian is given by:

$$H_0 = K + U_c + U_H + U_{\rm XC} + eEz + V_{\rm mag}^{\rm eff}(z). \qquad (1)$$

Here, K is the kinetic part (we use the parabolic approximation with heavy-hole effective masses),[43] U_c and U_H are the QW confinement and Hartree potentials,[44] and $-e$ is electron charge. $U_{\rm XC}$ is an exchange-correlation correction.[45] The z-direction is perpendicular to interfaces, i.e., to the growth direction. First, by diagonalizing H_0 and solving the Schrödinger equation self-consistently, we obtain the spin-polarized hole eigenfunctions, $\phi_n(z)$, and eigenenergies, $\varepsilon_{n,\mathbf{k}}$, for states with a wavevector $\mathbf{k}$ in a spin-polarized sub-band n. The area density of holes in the QW, $p_{\rm 2D}$, may be greater than that of Mn ions: some of holes originate not from Mn, but from doping in the barriers,[25] thus $p_{\rm 2D}$ and Mn density are our independent input parameters.

Our calculations use a series of input values of the Mn normalized magnetization $0 \le \langle M\rangle \le 1$ (in the δ layer) given by the fraction $m/10$ of the saturation (i.e., $\langle M\rangle = m/10$), where $m = 0, 1, \ldots, 10$. $V_{\rm mag}^{\rm eff}(z)$ is linearly dependent on $\langle M\rangle$:

$$V_{\rm mag}^{\rm eff}(z) = -N_0\beta x_{\rm Mn}\sigma\frac{5}{2}\langle M\rangle g(z), \qquad (2)$$

where N_0 is the cation density, $N_0\beta = -1.2$ eV is the exchange constant,[16] $x_{\rm Mn}$ is Mn content, $g(z) = 1$ if z lies inside the magnetic layer, and $g(z) = 0$ elsewhere. $V_{\rm mag}^{\rm eff}$ represents either a barrier for carrier spins aligned to the average magnetization ($\sigma = +1/2$), or a well for anti-aligned spins ($\sigma = -1/2$).

In the second step of our scheme, we use ϕ_n and $\varepsilon_{n,\mathbf{k}}$ to calculate magnetization-dependent corrections to energy, which are bilinear in the Mn-ion spins:

$$H_{\rm eff} = -\sum_{i\neq j}[(C_{ij}^{\uparrow\uparrow}+C_{ij}^{\downarrow\downarrow})S_i^3S_j^3+(C_{ij}^{\uparrow\downarrow}+C_{ij}^{\downarrow\uparrow})(S_i^1S_j^1+S_i^2S_j^2)], \qquad (3)$$

where the indices 1, 2 and 3 refer to three orthogonal axes, not necessarily the same as the x, y, and z directions, because we neglect spin-orbit coupling. The indices i, j run over Mn ions. However, we assume that axis 3 is, by means of an anisotropy of some origin, a favorable direction for magnetization. The exchange coefficients are given by:

$$C_{ij}^{\mu\nu} = -\sum_{n\in\mu}\sum_{n'\in\nu}\left(\frac{\beta}{2\tilde{A}}\right)^2 \times \phi_{n'}^*(z_i)\,\phi_n(z_i)\,\phi_n^*(z_j)\,\phi_{n'}(z_j)\,\chi^{n,n'}(\mathbf{R}_{ij}), \qquad (4)$$

where $\tilde{A}$ stands for the QW area in the xy-plane, and $\mathbf{R}_{ij} = \mathbf{R}_i - \mathbf{R}_j$. The summations on n and n' are restricted to sub-bands with the proper spin polarization, and the superscripts μ and ν refer to the hole spin up or down orientation (parallel or antiparallel with respect to the average Mn magnetization). Specifically, $C_{i,j}^{\uparrow,\downarrow}$ and $C_{i,j}^{\downarrow,\uparrow}$, represent the spin-flip terms. $\chi^{n,n'}(\mathbf{R}_{ij})$ is the real-space Fourier transform of the matrix element of the Lindhard function,[46]

$$\chi^{n,n'}(\mathbf{R}_{ij}) = \sum_{\mathbf{q}}\exp\left[-i\mathbf{q}\cdot\mathbf{R}_{ij}\right]\chi^{n,n'}(\mathbf{q}), \qquad (5)$$

with

$$\chi^{n,n'}(\mathbf{q}) = \sum_{\mathbf{k}}\frac{\theta(E_F-\varepsilon_{n,\mathbf{k}})-\theta(E_F-\varepsilon_{n',\mathbf{k}+\mathbf{q}})}{\varepsilon_{n',\mathbf{k}+\mathbf{q}}-\varepsilon_{n,\mathbf{k}}}. \qquad (6)$$

In Eqs. (5) and (6) $\mathbf{k}$ and $\mathbf{q}$ are in the 1st Brillouin zone, θ is the Heaviside step function, and E_F is the Fermi level. Further details of the method are described elsewhere.[44]

It is instructive to rewrite Eq. (3) to show that it naturally contains anisotropy:

$$H_{\rm eff} = -\sum_{i\neq j}J_{ij}\mathbf{S}_i\cdot\mathbf{S}_j - \sum_{i\neq j}A_{ij}S_i^3S_j^3, \qquad (7)$$

where $J_{ij} = (C_{ij}^{\uparrow\downarrow} + C_{ij}^{\downarrow\uparrow})$ and $A_{ij} = (C_{ij}^{\uparrow\uparrow} + C_{ij}^{\downarrow\downarrow} - C_{ij}^{\uparrow\downarrow} - C_{ij}^{\downarrow\uparrow})$. The first term in Eq. (7) is a Heisenberg interaction of two spins at sites i and j. The second term, an Ising interaction, reflects an anisotropy intrinsic to our model. As $\langle M\rangle \to 0$, A_{ij} vanishes, since the QW sub-bands become spin degenerate.[44]

We calculate $C_{ij}^{\mu\nu}$ for each set of ϕ_n and $\varepsilon_{n,\mathbf{k}}$ corresponding to one of the magnetization values m. These results, tabulated as $C_{ij}^{\mu\nu}(m)$, form the input to MC, which is the third stage of our approach. Employing the Metropolis algorithm,[47] we perform simulations for the classical spins $\mathbf{S}_i$ randomly distributed over cation sites with concentration $x_{\rm Mn}$. The randomness refers to both the site and to the initial (high-T) Mn-spin orientation. A small magnetic field $B_0 = 5$ mT, is applied in the z-direction imposing the growth direction as the easy axis for the magnetization [axis 3 in Eq. (3)]. A stepwise, slow cooling process is simulated, starting from $T > T_C$, and making sure that thermal equilibrium is reached at every consecutive temperature T. At high T, we use $C_{ij}^{\mu\nu}$ corresponding to $\langle M\rangle = m = 0$. Every time $\langle M\rangle$ increases to a higher fraction $m/10$ of the saturation value, the program switches to the corresponding set of $C_{ij}^{\mu\nu}(m)$.[44] More details of the MC procedure can be found in the Appendix.

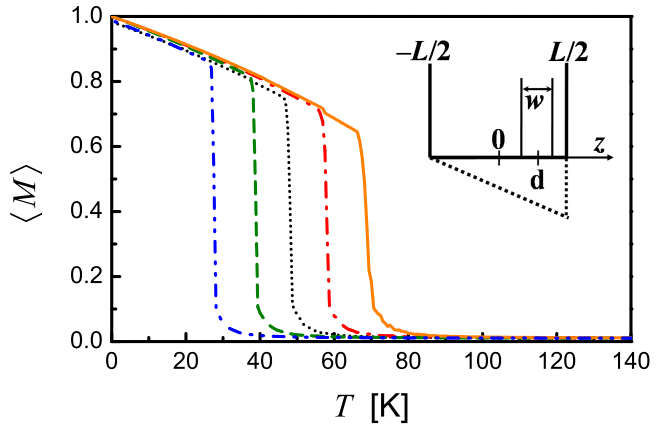

FIG. 1: (Color online) Temperature dependence of magnetization for: $E = -70$ kV/cm (dash-dot-dot), $E = -30$ kV/cm (dash), $E = 0$ (dot), $E = +30$ kV/cm (dash-dot), $E = +70$ kV/cm (solid). The magnetic layer of width w is displaced by $d = 0.1L$ from the QW center. The geometry is depicted in the inset, the broken line showing the band profile for $E > 0$.

III. RESULTS AND DISCUSSION

A complete phase diagram of (Ga,Mn)As for the full range of experimentally accessible values of p_{2D} and x_{Mn} is very complex.[48–50] It contains not only metal-insulator transitions, but also likely different types of magnetic ordering, implying that a single model is unlikely sufficient to provide a full description. Even a simplified situation, in which only x_{Mn} changes, is expected to lead to a nonmonotonic dependence of T_C on x_{Mn}. For example, a very low x_{Mn} would be insufficient to provide a robust ferromagnetic ordering, while a very high x_{Mn} would lead to strong Mn-Mn antiferromagnetic interactions, again detrimental for controllable ferromagnetism and high T_C. We therefore focus on the metallic phase of (Ga,Mn)As, consistent with parameters p_{2D} and x_{Mn} experimentally shown to yield relatively high T_C and a potential for highly controllable ferromagnetism.

The simulations are performed for a sample (Fig. 1) containing a (Ga,Mn)As δ-like layer of width $w = 8$ Å (three adjacent monolayers) and Mn concentration $x_{Mn} = 25\%$,[25] embedded in a GaAs QW of width $L = 60$ Å and area hole density $p_{2D} = 7.8 \cdot 10^{12}$ cm^{-2}. Periodic boundary conditions are applied along the x, y-directions. E field, applied along z, affects the charge distribution and changes the T_C. This effect is analyzed by placing the magnetic layer at different displacements d, measured from the center of the QW to the center of the δ-layer. Figure 1 shows $\langle M(T)\rangle$ for different values of the electric field E and for $d = 0.1L$. There is a sharp decrease of $\langle M(T)\rangle$ at T_C for all values of E. Comparing with previous simulations in thicker DMS layers,[44] this decrease is a consequence of the magnetic layer being close to the 2D limit. The calculation of the magnetic susceptibility (not shown) gives a clear determination of T_C in the ferromagnetic samples. We observe that $d > 0$ leads to an increase (decrease) of T_C as the E-field pointing to the right (left) increases, e.g., $E = 70$ kV/cm increases T_C by ~ 50 K with respect to the $E = -70$ kV/cm value.

To better understand the effects of the electric field on the transition temperature, $T_C(E)$, we note that the expression for $C_{ij}^{\mu\nu}$ in Eq. (4) depends on the wave function and thus, indirectly, on the volume carrier density, given by

$$p_{3D}(z) = \frac{m^*}{2\pi\hbar^2} \sum_n^{occ} (E_F - E_n) |\phi_n(z)|^2 , \qquad (8)$$

where E_n is the energy of the bottom of the sub-band n, i.e., $E_n = \varepsilon_{n,0}$. Usually, an increase of the carrier density leads to an increase of $C_{ij}^{\mu\nu}$.

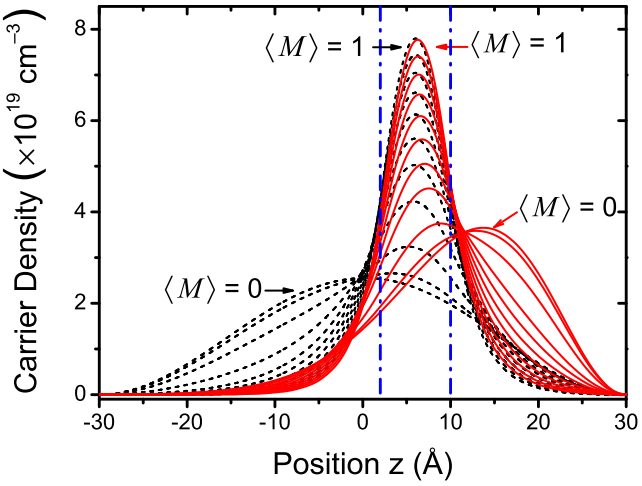

FIG. 2: (Color online) Carrier density distribution $p_{3D}(z)$ inside the QW for $E = 0$ (dashed) and $E = +200$ kV/cm (solid), and for various magnetizations $\langle M\rangle = 0,\ 0.1, \ldots,\ 1$. The center of the magnetic δ-layer of width w (left and right boundaries shown by vertical dash-dotted lines) is displaced from the QW center by $d = 0.1L$.

To illustrate the trends in the electric-field controlled ferromagnetism, we examine two different displacements of the magnetic layer: $d = 0.1L$ and $d = 0.43L$, in Fig. 2 and Fig. 3, respectively. With the latter value of d, the right barrier starts exactly at the right boundary of the δ-like layer. For each of these geometries, we show the effect of the applied E-field on the carrier density distribution, by choosing a specific value of $E = 200$ kV/cm. In this case, for both $d = 0.1L$ and $d = 0.43L$, we see that the peak position of the carrier density for $\langle M\rangle = 0$ does not coincide with the center of the magnetic layer. Following a simple interpretation of the strength of magnetic ordering and thus T_C (determined by the vanishing magnetization, i.e., $\langle M\rangle = 0$ curve), we expect that T_C should be related to degree of overlap of the carrier density with the magnetic layer. With an increase of E above 200kV/cm, the overlap of the carrier density with the δ-layer will decrease for $d = 0.1L$, while it will increase

for $d = 0.43L$. The two sample geometries considered in Figs. 2 and 3 are thus expected to yield opposite trends in E for T_C.

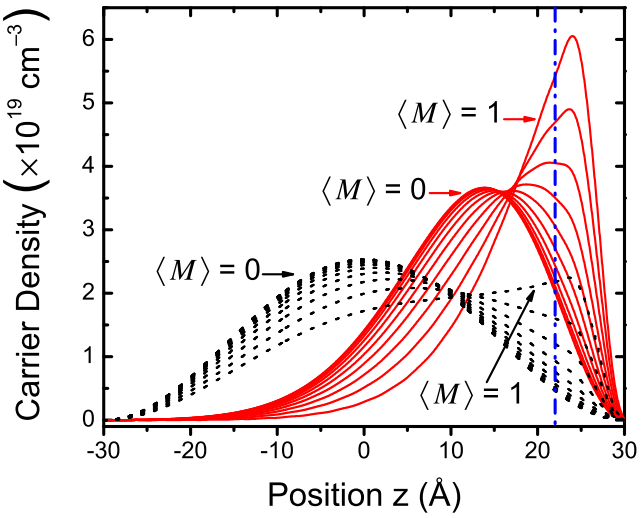

FIG. 3: (Color online) Carrier density distribution shown for $d = 0.43L$, with the remaining parameters same as in Fig. 2.

Two factors determine the carrier distribution for a given displacement: the electric field E and the mean-field potential $V_{\rm eff}^{\rm mag}$. A positive field pushes the holes to the right, shifting the hole distribution with respect to the δ-layer, and thus E controls the strength of indirect exchange. A proper choice of $E > 0$ will place the carriers in the vicinity of the layer at $\langle M\rangle = 0$, so that magnetic order appears at a temperature higher than that for $E = 0$. The second factor influencing $p_{\rm 3D}(z)$ is $V_{\rm eff}^{\rm mag}$, which increases with $\langle M\rangle$. This trend can be seen as an additional confinement for the majority-spin holes, resulting in a stronger localization in the δ-layer.

It would be desirable to have a simple picture providing the dependence between the carrier density $p_{\rm 3D}$ and T_C, for example, by evaluating $p_{\rm 3D}\,(z)$ for $\langle M\rangle = 0$ averaged over the magnetic δ-layer, which is readily available from the information provided in Figs. 2 and 3. However, recalling that the exchange coefficients in Eq. (4) are not just simply a function of carrier density, suggests that such an interpretation may not be sufficiently accurate and performing the MC simulations to elucidate various trends in T_C is indeed needed.

Figure 4 shows T_C obtained from MC simulations with several E values for various displacements d, including a direct comparison for the two geometries in Figs. 2 and 3 (given by full circle and star curves, respectively). Specifically, we see that the previously anticipated opposite trends, for $d = 0.1L$ and $d = 0.43L$, on T_C with $E > 200$ kV/cm are approximately satisfied. For the centered layer ($d = 0$), the application of an electric field reduces T_C, because E moves the carriers away from the layer. However, for the other d's, the E-field brings the carriers into the δ-layer up to a certain intensity, when

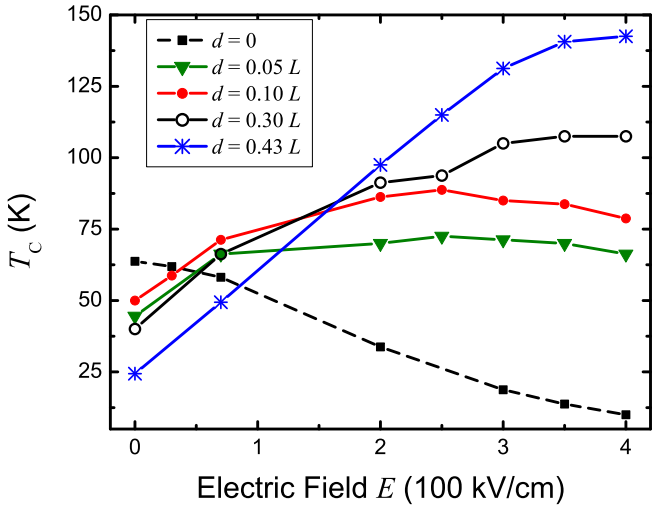

FIG. 4: (Color online) Dependence of the Curie temperature, T_C, on electric field for various off-center displacements d.

T_C reaches a maximum. The E-field giving the maximum T_C, increases with d. Having explained the usefulness of studying the variation of carrier density, we note again that $p_{\rm 3D}$ alone can not be used to predict T_C quantitatively. For example, a comparison of the $p_{\rm 3D}$ values averaged over the δ-layer for $d = 0.1L$ and $d = 0.43L$ at $E = 200$ kV/cm on one hand (red lines for $\langle M\rangle = 0$ in Figs. 2 and 3), with the corresponding T_C values in Fig. 4 on the other hand, shows different trends. Thus, as previously mentioned, our MC simulations are necessary to determine T_C.

The above results suggest the feasibility of highly-tunable ferromagnetic ordering for an optimized d/L ratio (in contrast, for $d/L = 0.05$ there is only a modest change in T_C, for a wide range of E). Specifically, for $d/L = 0.43$ the corresponding change $\Delta T_C > 100$ K is an order of magnitude larger than the previously measured maximum change in DMS.[18–20] This large ΔT_C arises from two factors: First, the $\langle M\rangle = 0$ hole density in the δ layer, and consequently T_C, are relatively small for small E. Second, unlike for other displacements d, application of large E for $d = 0.43L$ does not result in an 'overshoot' of hole density, because the right boundaries of the magnetic layer and of the QW coincide in this case. This difference can be seen by comparing the $\langle M\rangle = 0$ solid curves in Fig. 2 and Fig. 3. The absence of 'overshoot' leads to the relatively high T_C for high E.

The required fields in Fig. 4 are less than those for dielectric breakdown of the gate insulator in FETs, $\sim$ MV/cm. Furthermore, with the recent gating advances achieved by incorporating an electrochemical cell into the FETs,[15,17,19] in a device known as the electric double-layer transistor (EDLT), the breakdown voltages can attain 10 MV/cm.[14]

The impossibility of having a ferromagnetic order in 2D systems without an anisotropy was discussed previously.[38,51] On the other hand, the ferromagnetism

exists in very thin (digital) layers of (Ga,Mn)As, therefore a model intended to explain magnetic behavior of these systems has to include anisotropy [recall Eq. (7)]. However, the question about the effect of an anisotropy persisting even above T_C remains open. To explore this possibility, we performed some simulations decreasing the magnetic field, B_0, from the standard value $B_0 = 5$ mT used in Figs. 1, 4, and 6. In Fig. 5, for $B_0 < 5$ mT, we obtain partial magnetization at $T = 0$, but ferromagnetism persists (dash-dot, triangles and dash-dot-dot lines). Suppression of anisotropy, [$A_{ij} = 0$ in Eq. (7)], results in a very unusual $\langle M(T)\rangle$, where strong oscillations appear (dotted and solid lines). This implies that the anisotropy A_{ij}, inherent to our model, is crucial for obtaining ferromagnetism. The influence of anisotropy can be examined by comparing the $A_{ij} = 0$ and $A_{ij} \neq 0$ results obtained with the small, $B_0 = 5$ mT, magnetic field, corresponding to the the solid and dash-dot curves in Fig. 5. From these findings we see that our MC simulation is not suitable to treat the case of vanishing anisotropy, although the absence of anisotropy leads to a strange magnetic order, if any, as shown in Fig. 5 (solid line). The difficulties when we eliminate both B_0 and A_{ij} are related to the fact that magnetization fluctuations in the MC process lead to some anisotropic order in the magnetic dipole orientation, and this induces a magnetic order in the stepwise slow cooling process.

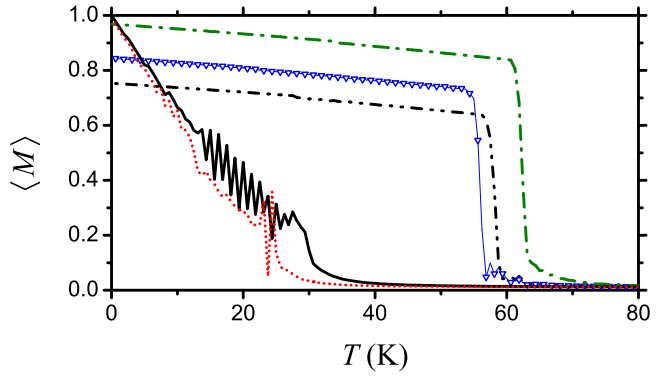

FIG. 5: (Color online) Temperature dependence of magnetization for $E = d = 0$ and different external magnetic fields: $B_0 = 0$ (dash-dot-dot), $B_0 = 0.05$ mT (triangles), $B_0 = 5$ mT (dash-dot). The dotted (for $B_0 = 0$) and solid (for $B_0 = 5$ mT) curves are for $A_{ij} = 0$ in Eq. (7).

While our results are motivated by the use of (Ga,Mn)As-based parameters[16] and experiments on magnetic QWs,[18,25] they could also indicate trends relevant for other DMS and optimized geometries by varying the displacement d. A useful indication of the E-field controlled magnetism is the highest relative change (increase) of T_C obtained by the application of the electric field ($E \geq 0$) i.e., $\Delta T_C/T_C(0) \equiv [T_C(E_0) - T_C(0)]/T_C(0)$, where E_0 is the optimal field which yields the highest T_C. The corresponding results, including additional displacements complementing those in Fig. 4, are given in Fig. 6. The sharp rise of T_C with E for large d is a consequence of the charge distribution, which is occupying a region away from the δ-layer center, when $E = 0$. As the E increases, it pushes the charge distribution onto the δ-layer, resulting in a significant increase of T_C, until it reaches the highest T_C at E_0. Above E_0, some of the carriers leave the δ-layer and reside close to the right QW boundary (cf. inset in Fig. 1). The larger the displacement d, the higher the optimal field E_0, see dashed line in Fig. 6.

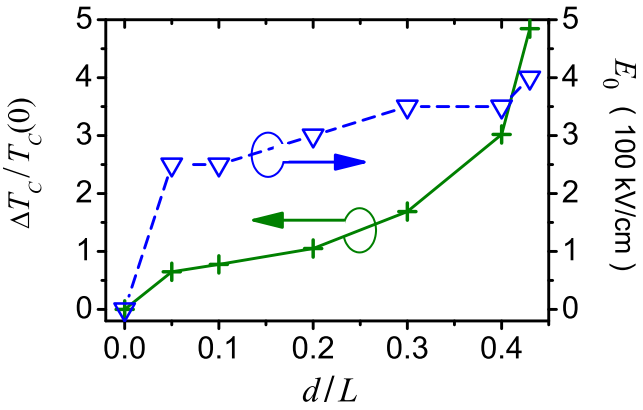

FIG. 6: (Color online) Highest relative change of T_C induced by E for different d (solid line), and the corresponding optimal E_0 (dashed line). The connecting lines are only eye-guides.

IV. CONCLUSIONS

In this work we have used MC simulations to optimize the placement of a thin magnetic Mn-layer in a (Ga,As) QW in order to achieve large E-field controlled changes of T_C. While our findings predict an order of magnitude higher ΔT_C than the previously measured values,[18–20] we expect that even further improvements are possible. For example, the required E-fields are substantially smaller than those attainable in recently employed EDLTs,[15,17,20] and our calculated $T_C(E = 0)$ remain smaller than those reported in magnetic QWs.[18–20]

Beyond (Ga,Mn)As, similar gating studies could help elucidate the mechanism responsible for magnetic ordering in other DMS systems.[17] It would also be important to consider magnetic quantum dots in which addition of a single carrier can already have an important ramifications on magnetic ordering.[52–59] Analogous to our considerations of changing magnetization at a constant total carrier density, in magnetic quantum dots it may also be possible to realize gate-controlled change of magnetization at a fixed number of carriers.[60,61]

Gating experiments could also offer enhanced functionality for spintronic devices.[3] The prediction of magnetic bipolar transistor[62] has been recently demonstrated based on (In,Mn)As,[63] the first DMS in which gating was

realized.[2] An optimized gating in such devices could offer large changes in the signal amplification, even without the currently required strong magnetic fields.[63]

Acknowledgments

This work was supported by the DOE-BES DE-SC0004890, US ONR N0000140610123, AFOSR-DCT FA9550-09-1-0493,NSF-ECCS CAREER 054782, the Brazil CNPq, and FAPEMIG.

Appendix: Calculation scheme

Our calculation scheme consists of three main steps:
(i) We perform a self-consistent calculation of the electronic structure (ϕ_n and $\varepsilon_{n,\mathbf{k}}$) for 11 equidistant values of the normalized magnetization ($m = 0, 1, \ldots, 10$).
(ii) From the electronic structure we calculate coupling coefficients $C_{i,j}^{\mu,\nu}$ (which determine the exchange integrals $J_{i,j}$ and $A_{i,j}$). These coefficients are tabulated for $m = 0, 1, \ldots, 10$ as $C_{i,j}^{\mu,\nu}(m)$.
(iii) We run the Monte Carlo simulation, starting at a high temperature T well above T_C. At this initial T we use $\langle M\rangle = 0$, i.e., the $C_{i,j}^{\mu,\nu}(m = 0)$ table with exchange integrals. Next, we start reducing T. If, at any value of T, $\langle M\rangle$ increases to be closer to $\langle M\rangle = 0.1$ than to $\langle M\rangle = 0$ (i.e., closer to $m = 1$ than to $m = 0$), then the program switches to the corresponding table $C_{i,j}^{\mu,\nu}(m = 1)$. This table is used until at an even lower temperature, the magnetization increases to a value closer to $\langle M\rangle = 0.2$ (i.e., $m = 2$). At this point, the program switches to the table $C_{i,j}^{\mu,\nu}(m = 2)$, and so on.

This calculation scheme circumvents the need of calculating the electronic structure for each temperature considered in the MC simulation.

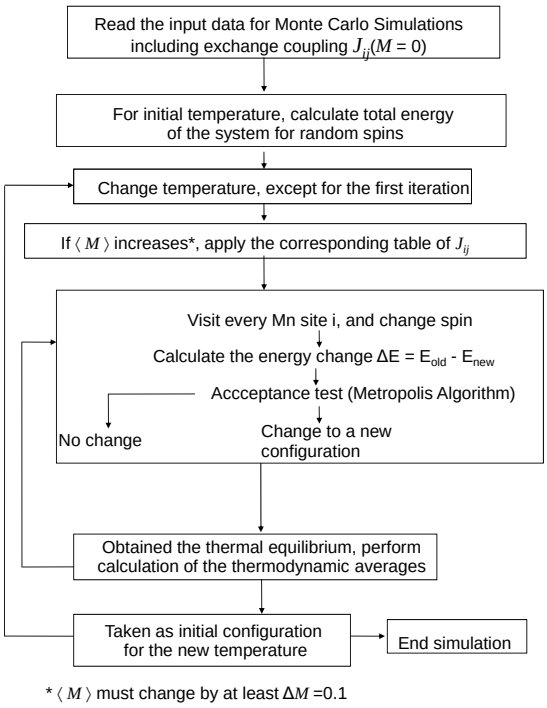

FIG. 7: Schematic representation of the algorithm used for implementing the Monte Carlo simulation.

[1] L. G. F. Filho, I. C. da Cunha Lima, and A. Troper, Semicond. Sci. Technol. **12**, 1592 (1997).
[2] H. Ohno et al., Nature **408**, 944 (2000).
[3] I. Žutić, J. Fabian, and S. Das Sarma, Rev. Mod. Phys. **76**, 323 (2004).
[4] S. Koshihara et al., Phys. Rev. Lett. **78**, 4617 (1997).
[5] A. G. Petukhov, I. Žutić, and S. C. Erwin, Phys. Rev. Lett. **99**, 257202 (2007).
[6] M. J. Calderón and S. Das Sarma, Phys. Rev. B **75**, 235203 (2007).
[7] V. Krivoruchko et al., J. Magn. Magn. Mater. **322**, 915 (2010).
[8] C. H. Ahn et al., Rev. Mod. Phys. **78**, 1185 (2006).
[9] S. C. Erwin and A. G. Petukhov, Phys. Rev. Lett. **89**, 227201 (2002).
[10] T. Jungwirth et al., Phys. Rev. B **76**, 125206 (2007).
[11] E. Dias Cabral, I. C. da Cunha Lima, M. A. Boselli, and A. T. da Cunha Lima, Appl. Phys. Lett. **93**, 112110 (2008).
[12] B. L. Sheu et al., Phys. Rev. Lett. **99**, 227205 (2007).
[13] M. Sawicki et al., Nat. Phys. **6**, 22 (2010).
[14] R. Kötz and M. Carlen, Electrochim. Acta **45**, 2483 (2000).
[15] K. Ueno et al., Nat. Mater. **7**, 855 (2008).
[16] T. Jungwirth, J. Sinova, J. Mašek, J. Kučera, and A. H. MacDonald, Rev. Mod. Phys. **78**, 809 (2006).
[17] A notable exception is the Co-doped TiO_2, with recently reported room temperature control of ferromagnetism, Y. Yamada, K. Ueno, T. Fukumura, H. T. Yuan, H. Shimotani, Y. Iwasa, L. Gu, S. Tsukimoto, Y. Ikuhara, and M. Kawasaki, Science **332**, 1065 (2011); I. Žutić and J. Cerne, Science **332**, 1040 (2011).
[18] A. M. Nazmul, S. Kobayashi, S. Sugahara, and M. Tanaka, Jpn. J. Appl. Phys. **43**, L233 (2004).
[19] Y. Nishitani et al., Phys. Rev. B **81**, 045208 (2010).
[20] M. Endo et al., Appl. Phys. Lett. **96**, 022515 (2010).
[21] D. Chiba, F. Matsukura, and H. Ohno, Appl. Phys. Lett. **89**, 162505 (2006).
[22] M. H. S. Owen et al., New J. Phys. **11**, 023008 (2009).
[23] X. Chen et al., Appl. Phys. Lett. **81**, 511 (2002), the authors attribute, to some extent, the high T_C value to 2D islands of MnSb.
[24] S. R. Dunsiger et al., Nat. Mater. **9**, 299 (2010).
[25] A. M. Nazmul, T. Amemiya, Y. Shuto, S. Sugahara, and M. Tanaka, Phys. Rev. Lett. **95**, 017201 (2005).
[26] V. Novák et al., Phys. Rev. Lett. **101**, 077201 (2008).
[27] L. Chen et al., Appl. Phys. Lett. **95**, 182505 (2009).
[28] N. Kim, S. Lee, T. Kang, and H. Kim, Phys. Rev. B **69**, 115308 (2004).
[29] B. Lv et al., Appl. Phys. Lett. **90**, 142513 (2007).
[30] C. Timm, J. Phys.: Condens. Matter **15**, R1865 (2003).
[31] J. Schliemann, J. König, H.-H. Lin, and A. H. MacDonald, Appl. Phys. Lett. **78**, 1550 (2001).
[32] K. Sato, H. Katayama-Yoshida, and P. H. Dederichs, Jpn. J. Appl. Phys. **44**, L948 (2005).
[33] R. Bouzerar, G. Bouzerar, and T. Ziman, Phys. Rev. B **73**, 024411 (2006).
[34] G. Alvarez, M. Mayr, and E. Dagotto, Phys. Rev. Lett. **89**, 277202 (2002).
[35] J. Schliemann, J. König, and A. MacDonald, Phys. Rev. B **64**, 165201 (2001).
[36] L. Brey and G. Gómez-Santos, Phys. Rev. B **68**, 115206 (2003).
[37] M. Kennett, M. Berciu, and R. Bhatt, Phys. Rev. B **66**, 045207 (2002).
[38] D. Priour, E. Hwang, and S. Das Sarma, Phys. Rev. Lett. **95**, 037201 (2005).
[39] D. Kechrakos, N. Papanikolaou, K. Trohidou, and T. Dietl, Phys. Rev. Lett. **94**, 127201 (2005).
[40] A. Lipińska et al., Phys. Rev. B **79**, 235322 (2009).
[41] M. A. Boselli, I. C. da Cunha Lima, J. R. Leite, A. Troper, and A. Ghazali, Appl. Phys. Lett. **84**, 1138 (2004).
[42] A. Nazmul, S. Sugahara, and M. Tanaka, Phys. Rev. B **67**, 241308 (2003). Moreover, placing individual Mn can be done with atomic scale precision using a STM tip: D. Kitchen *et al.,* Nature (London) **442**, 436 (2006) and C. F. Hirjibehedin *et al.,* Science **312**, 1021 (2006). This technique can have significant implications for magnetic ordering in Mn-doped Quantum Dots, see for example R. Oszwałdowski *et al.,* Phys. Rev. Lett. **106**, 177201 (2011).
[43] A. Twardowski and C. Hermann, Phys. Rev. B **35**, 8144 (1987), we take into account the effective mass anisotropy, $m_{xy} = 0.11$, $m_z = 0.37$.
[44] M. A. Boselli, I. C. da Cunha Lima, and A. Ghazali, Phys. Rev. B **68**, 085319 (2003).
[45] The exchange in $U_{\rm XC}$ is not related to the d-electrons in Mn, but to the 2D holes; $U_{\rm XC}(\mathbf{r}) = -(e^2/4\pi\epsilon_0)[3n(\mathbf{r})/\pi]^{1/3}[1 + 0.7734t\ln(1 + 1/t)]$, where $t = r_s/21$, $r_s = (4\pi a_B^3 n/3)^{-1/3}$, and a_B is the Bohr radius, cf. Eq. (2.74) in Fundamentals of Semiconductor Physics and Devices, R. Enderlein and N. J. Horing, (World Scientific, Singapore 1997).
[46] A. A. Abrikosov, L. P. Gorkov, and I. Dzyaloshinski, *Methods of Quantum Field Theory in Statistical Physics*, Dover, 1975.
[47] D. P. Landau and K. Binder, *A Guide to Monte Carlo Simulations in Statistical Physics*, Cambridge Univ. Press., 2009, p. 70.
[48] E. J. R. de Oliveira, I. C. da Cunha Lima, E. Dias Cabral and M. A. Boselli, J. Appl. Phys. **109**, 023709 (2011).
[49] C. Timm, in *Handbook of Spin Transport and Magnetism*, edited by E. Y. Tsymbal and I. Žutić, Taylor & Francis (2011, in press), pp. 385-404.
[50] A. Van Esch *et al.*, Phys. Rev. B **56**, 13103 (1997).
[51] A. Gelfert and W. Nolting, Phys. Status Solidi B **217**, 805 (2000).
[52] J. Seufert *et al.*, Phys. Rev. Lett. **88**, 027402 (2002).
[53] L. Besombes *et al.*, Phys. Rev. Lett. **93**, 207403 (2004).
[54] J. Fernández-Rossier and L. Brey, Phys. Rev. Lett. **93**, 117201 (2004), J. Fernández-Rossier, Phys. Rev. B **73**, 045301 (2006).
[55] A. O. Govorov, Phys. Rev. B **72**, 075358 (2005); Phys. Rev. B **72**, 075359 (2005).
[56] N. T. T. Nguyen and F. M. Peeters, Phys. Rev. B **78**, 045321 (2008).
[57] R. Beaulac *et al.*, Science **325**, 973 (2009).
[58] S. T. Ochsenbein *et al.*, Nature Nanotech. **4**, 681 (2009); I. Žutić and A. G. Petukhov, Nature Nanotech. **4**, 623 (2009).
[59] I. R Sellers *et al.*, Phys. Rev. B **82**, 195320 (2010).
[60] R. M. Abolfath, P. Hawrylak, and I. Žutić Phys. Rev. Lett. **98**, 207203 (2007).
[61] R. M. Abolfath, A. G. Petukhov, and I. Žutić Phys. Rev. Lett. **101**, 207202 (2008).

[62] J. Fabian, I. Žutić, and S. Das Sarma, Appl. Phys. Lett. **84**, 85 (2004); J. Fabian and I. Zutić, Phys. Rev. B **69**, 115314 (2004).

[63] N. Rangaraju, J. A. Peters, and B. W. Wessels, Phys. Rev. Lett. **105**, 117202 (2010).